IEEE Access
Multidisciplinary ⋮ Rapid Review ⋮ Open Access Journal

Received 8 April 2024, accepted 6 May 2024, date of publication 13 May 2024, date of current version 20 May 2024.

Digital Object Identifier 10.1109/ACCESS.2024.3399814

RESEARCH ARTICLE

Singly-Fed Large Frequency Ratio Composite Dielectric Resonator Antenna for sub-6 GHz and mm-Wave 5G Applications

ASADULLAH[1], MUHAMMAD UMAR KHAN[1], (Member, IEEE), AWAB MUHAMMAD[1], MOHAMMAD S. SHARAWI[2,3], (Fellow, IEEE), AND MOATH ALATHBAH[4]

[1]School of Electrical Engineering and Computer Science, National University of Sciences and Technology (NUST), Islamabad 44000, Pakistan
[2]Poly-Grames Research Center, Electrical Engineering Department, Polytechnique Montréal, Montreal, QC H3C 3A7, Canada
[3]Blue Origin LLC, Kent, WA 98032, USA
[4]Department of Electrical Engineering, College of Engineering, King Saud University, Riyadh 11421, Saudi Arabia

Corresponding author: Muhammad Umar Khan (umar.khan@seecs.edu.pk)

This work was supported by King Saud University, Riyadh, Saudi Arabia, through the Researchers Supporting Project under Grant RSPD2024R868.

ABSTRACT A dielectric resonator antenna (DRA) is proposed for dual-band resonance for the mid-band (sub-6 GHz) and the high-band (millimeter-wave) 5G applications. The proposed composite DRA consists of an annular dielectric radiator concentrically integrated with a high-permittivity cylindrical DRA to realize resonance at two distinct frequencies with large frequency ratio. The impact of composition of two distinct dielectric materials on the radiation in both bands is analyzed taking into account the effective permittivity of the composite structure. The composite DRA is excited with single Co-planar Waveguide (CPW). The proposed DRA offers resonance at 4.44 GHz in the mid-band and 27.92 GHz in the high-band. The radiation characteristics demonstrate broadside radiation pattern having 6.8 dBi and 4.3 dBi of gain in both bands respectively. The efficiency of the DRA is observed to be 87.1% and 84.71% in the sub-6 GHz and mm-wave bands, respectively. The radiation characteristics make the proposed composite DRA a potential design for numerous 5G applications.

INDEX TERMS Dual-band DRA, large frequency ratio, singly-fed DRA, 5G antenna, composite DRA.

I. INTRODUCTION

The microwave spectrum faces congestion due to the ever-increasing capacity demand pushed by rapid advancements in computing systems and communication technology [1], [2]. In order to accommodate the increasing demand of the capacity and avoid the congestion in microwave spectrum, millimeter-wave (mm-wave) frequency band is utilized for 5G communication. The mm-wave offers significantly higher data-rate by exploiting wider channel bandwidth. The mm-wave based 5G communication allows utilization of up to 500 MHz of channel bandwidth as compared to the 20 MHz bandwidth in the 4G communication system. Moreover, the recent advancements in the semiconductor technology have also enabled CMOS to operate on the mm-wave spectrum thus allowing the base station and mobile equipment manufacturers to produce cost effective mm-wave based 5G systems [3], [4].

However, the mm-wave propagation is affected by obstructions, atmospheric absorption, and attenuation specially in urban areas. Thus, the mm-wave offers effective communication only within a few hundred meters of the range [5]. For long-range communication, wireless systems still inevitably rely on microwave-based communication. Achieving multi-band operations with a large frequency ratio using single radiator and single feed is a formidable task. The critical challenges in the design and characterization of dual-band large frequency ratio antenna include realization of sufficient radiation efficiency in both bands and an efficient feeding mechanism that ensures ease of integration

The associate editor coordinating the review of this manuscript and approving it for publication was Ravi Kumar Gangwar.

with the underlying systems. Several antenna designs have been proposed to meet the dual-band requirement in both the microwave and mm-wave frequency bands. Commonly, a conducting radiator such as monopole, patch or slot radiator is employed to resonate at distinct frequency bands [6], [7], [8], [9], [10]. However, metallic radiators offer narrow bandwidth, less efficiency and higher conducting losses specially at the mm-wave band. Whereas, dielectric resonator antennas (DRAs) are recognized for their ability to provide more efficient resonance, wideband radiation characteristics, more design flexibility and support for a wide variety of excitation techniques which allows them to be easily integrated into variety of systems [11], [12]. The DRAs have gained significant attention as potential choices for dual-band applications [13], [14], [15], [16], [17], [18], [19]. A 3D-printed cylindrical DRA was combined with dielectric lens and a dielectric rod for dual wide-band resonance [20]. The cylindrical DRA and lens resonate at sub-6 GHz band with fractional bandwidth of 21%, while the dielectric rod acts as an mm-wave resonator with 26.2% bandwidth. The peak gain attained by the antenna was 6.4 dBi in the lower band and 12.7 dBi in the higher band. A rectangular DRA (rDRA) for dual-band resonance was proposed by [21]. The rDRA was designed for microwave band resonance (2.4 GHz) and a conducting groove was embedded to form a Fabry–Perot resonator antenna (FPRA) for mm-wave band (24 GHz). The antenna was excited with two distinct ports for microwave and mm-wave bands. A hollow DRA annexed with FPRA was proposed for dual-frequency resonance [22]. Dual-port feed was used to excite the antenna to realize dual-band resonance at 2.4 GHz and 24 GHz by positioning the FPRA and air gap of the hollow region of the DRA. Microstrip feed was used to excite the DRA, and WR-34 waveguide was used to feed FPRA. Reference [23] introduced encapsulated DRAs, where smaller DRAs with high permittivity were embedded within larger DRAs with lower permittivity, which enabled efficient radiation at two broadly separated frequency bands. The antenna covered sub-6 GHz resonating at 3.2 GHz and the mm-wave band for 5G and beyond applications with resonance at 31.5 GHz. 3D printing through filament deposition method was used to create the dual wide-band E-DRAs, which utilize a 5-element array of small cylindrical DRAs for mm-wave bands and larger cDRA with a dielectric lens for high-gain radiation. A 5-element array of high-permittivity radiators was added to achieve beam-switching capability. The antenna had separate microstrip feeds for low-frequency and high-frequency resonances. Another DRA for large frequency ratio dual-band applications was presented in [24]. The antenna was dual-fed and consisted of a slot radiator and substrate integrated DRA to offer resonance in the sub-6 GHz frequency band and the mm-wave band. A hollow conducting patch was embedded with the slot antenna to achieve high frequency resonance. Both low-frequency and high-frequency antennas were excited using slot coupled feeding mechanism embedded under a secondary substrate beneath the main substrate. Recently, [25] proposed a multi-port integrated large-frequency ratio DRA, comprising a MIMO and an array. The MIMO antenna was based on 2 dielectric elements for sub-6 GHz resonance and 4 array elements covering mm-wave band. However, the DRA array was fed through a 1×4 grounded co-planar waveguide (GCPW) power divider and the MIMO elements were excited with separate GCPW feedlines.

The dual-band large frequency ratio DRAs in the known literature are limited to using multi-port excitations involving different types of feeding mechanisms including microstrip, slot-coupled, and the waveguide. However, the singly-fed DRAs have been proposed only for small frequency ratio resonances. A singly-fed rectangular DRA with diagonal groove and two opposite vertices chamfered was proposed for small dual-band operation with small frequency ratio [26]. The slot coupled feeding was used to excite the DRA for resonance at 1.58 GHz and 2.44 GHz. A similar approach for the excitation of a truncated cylindrical DRA was utilized to achieve resonance at 5.19 GHz and 9.13 GHz [18].

In this paper, a singly-fed dual-band composite DRA with large frequency ratio is proposed. The proposed DRA exploits the combination of two distinct dielectric structures to form a composite structure that covers both sub-6 GHz and mm-wave bands for 5G communication. Composite DRA is excited using a single port CPW feed. The proposed dual-band DRA for 5G exhibits resonance in both n79 and n261 bands. The large frequency ratio offered by the proposed DRA ensures compatibility with a diverse range of applications in 5G. sub-6 GHz applications include Enhanced Mobile Broadband (eMBB) for reliable communication and Massive Machine-Type Communication (mMTC) within the Internet of Things (IoT) framework. Resonance in the mm-wave band (n261) at 27.92 GHz makes it suitable for low-latency applications like Ultra-Reliable Low Latency Communications (URLLC) and Fixed Wireless Access (FWA).

The rest of the paper is arranged as follows: the antenna design evolution is presented in section II, which also describes the phases of the design to achieve the final proposed design of the composite DRA. Section III presents the radiation characteristics of the simulated and fabricated prototype. A brief comparison between the proposed composite DRA and the state-of-the-art is also presented in the same section. The conclusion is presented in section IV.

II. ANTENNA DESIGN EVOLUTION

The design process is aimed to utilize a combination of distinct dielectric radiators to achieve resonance in two widely separated frequencies which cover both the mid-band (sub-6 GHz) and the high-band (mm-wave). Rogers RT/Droid 5870 having $\varepsilon_r = 2.33$, 0.787 mm thickness and the loss tangent of 5×10^{-4} is used as the substrate. The chosen substrate is well suited for applications involving large frequency ratio due to its consistent dielectric

constant and the loss tangent for frequency spectrum ranging up to 40 GHz. The design process involves two iterations which are aimed to achieve dual-band resonance. In the first iteration, an annular dielectric resonator is designed to realize the low frequency resonance. In the second iteration, a cylindrical DRA composed of a higher dielectric constant material is embedded concentrically in the annular antenna. The succeeding subsection presents the methodology for design of the annular DRA.

A. ANNULAR DRA DESIGN

In the first phase, the annular DRA is constructed using white marble as its dielectric material. The dielectric properties of the marble may vary depending on its composition of elements. White marble typically contains a composition of calcium oxide, magnesium oxide and iron. It consists of a high percentage of calcite mineral as compared to other commonly available marbles such as grey, brown and tiger-skin marble. The latter ones consist of higher concentration of carbon, aluminum and manganese oxides which results in very high permittivity making them unsuitable for the composite DRA [27]. White marble possesses the relative permittivity $\varepsilon_r = 8.3$, loss tangent of $5 \times 10^{-4,}$ and the relative permeability $\mu_r = 1$ [28].

Resonant frequency of the annular DRA is approximated using the cavity model [29]. The walls of the annular DRA are approximated by magnetic boundaries. The wave function for the fundamental mode $TM_{01\delta}$ of the approximated cavity can be expressed as:

$$\psi = J_1\left(\frac{X\rho}{a}\right) cos\varphi \cos\frac{z\pi}{2d} \tag{1}$$

where J_1 is the Bessel function of the first kind, a is the outer radius, d is the height of the DRA, φ and ρ are the cylindrical coordinates of the feed.

The parameter X is the root of the Bessel's equation of the first kind. The mathematical expression for the resonant frequency of the fundamental resonant mode $TM_{01\delta}$ is written as:

$$f_{TM_{01\delta}} = \frac{c_o}{2\pi a\sqrt{\varepsilon_r}}\sqrt{X^2 + \left(\frac{\pi a}{2d}\right)^2} \tag{2}$$

The resonance frequency of both cylindrical as well as annular DRAs can be evaluated using (2). The value of X varies with the ratio of the inner radius to the outer radius of the annular structure. Therefore, the cylindrical DRA is considered as a special case of annular DRA where the ratio of inner to outer radius is zero [29]. Fig. 1 presents the structure of the annular marble DRA.

Design attributes of the annular DRA are shown in Table. 1. For the given parameters of the proposed annular DRA, the ratio of inner radius b to outer radius a, b/a is 0.68 and the root X holds the value of 9.7. The resonant frequency is calculated using (2) and is found to be 7.41 GHz. The resonant frequency is higher than the targeted frequency for sub-6 GHz 5G band. Nevertheless, the deliberate adjustment of the resonant frequency is made higher than the desired frequency. This deliberate alteration anticipates that, in the second phase of DRA design, the incorporation of a high permittivity center DR would effectively alter the resonant frequency.

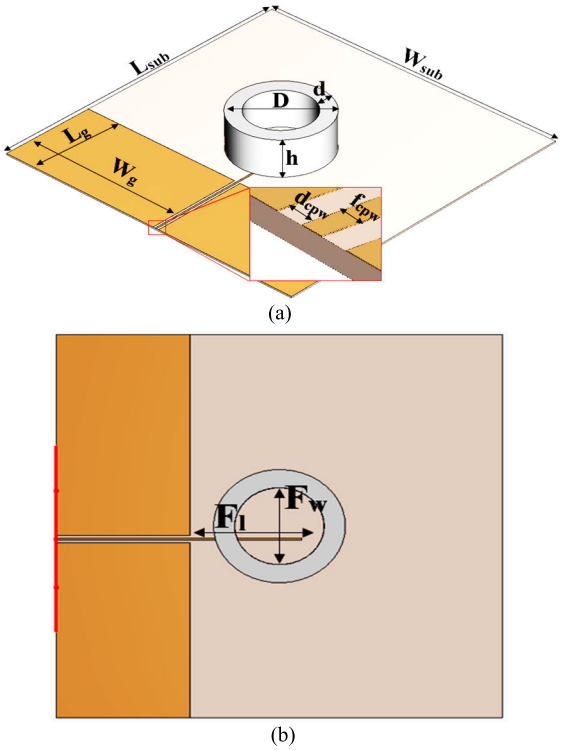

FIGURE 1. Geometric structure of the proposed annular DRA (a) side view (b) top view.

TABLE 1. Design parameters of DRA.

Parameter	Value (mm)
D	44
h	20
W_g	77
L_g	45
L_{sub}, W_{sub}	150
F_{cpw}	0.4
d_{cpw}	0.25
d	7
F_l	17
F_w	35

B. COMPOSITE DRA DESIGN

In the second phase, the annular DRA is integrated with high permittivity cylindrical structure. The geometric representation of the composite DRA is presented in Fig. 2.

The DRAs made from materials possessing high dielectric constant are generally more efficient, robust and low-profile structures that are used for wide range of applications [30], [31], [32], [33]. Commonly used high permittivity dielectric materials are typically composed of ceramic materials that

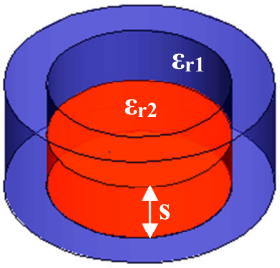

FIGURE 2. Geometry of composite DRA, s=10mm, εr1= 8.3 and εr2 = 12.94.

include various types of titanates such as barium titanate, strontium titanate, lead zirconate titanate, calcium titanate and magnesium titanate [34], [35], [36], [37]. Ceramic materials are a suitable choice for the applications requiring high permittivity materials. However, their dielectric properties are more susceptible to variations in frequency. This nature makes them inappropriate for applications involving multi-band resonance with large frequency ratio. Furthermore, the titanate based ceramic materials are temperature sensitive and possess spontaneous polarization making them unstable and less efficient [38]. Gallium Arsenide (GaAs) is used to construct the inner DR of the proposed antenna. It is a semi-conductor having high bandgap energy. The higher electron mobility and wide bandgap of GaAs make it more suitable for both microwave and the mm-wave band applications.

Addition of the high permittivity structure alters the effective permittivity ε_{eff} of the radiator. The substance and the dimensions of the high permittivity structure are chosen such that ε_{eff} of the composite DRA becomes approximately equal to the permittivity of marble cylindrical DRA. This approximation will be considered for evaluating the resonant frequency of the proposed composite DRA. The effective permittivity of the composite material can be defined as the sum of products of relative permittivity and the fractional volume of each material [39]. The effective permittivity of the composite DRA can be evaluated using:

$$\varepsilon_{eff} = \varepsilon_a f_a + \varepsilon_m f_m + \varepsilon_g f_g \tag{3}$$

where the subscripts a, m and g represent the air, marble and GaAs material and the f represents the fractional volume of each material. The computed effective permittivity of the composite DRA stands at 7.67. However, (3) does not take into account the variations in frequency. For large frequency-ratio applications, it is crucial to consider the frequency dependency of the effective permittivity of the composite DRA. In order to understand the impact of varying frequency, parametric analysis of the effective permittivity for different volumes of GaAs in the composite DRA is carried out using the two-port waveguide method [40]. Fig. 3 depicts the permittivity profiles of the composite DRA for various volumes of GaAs based DR.

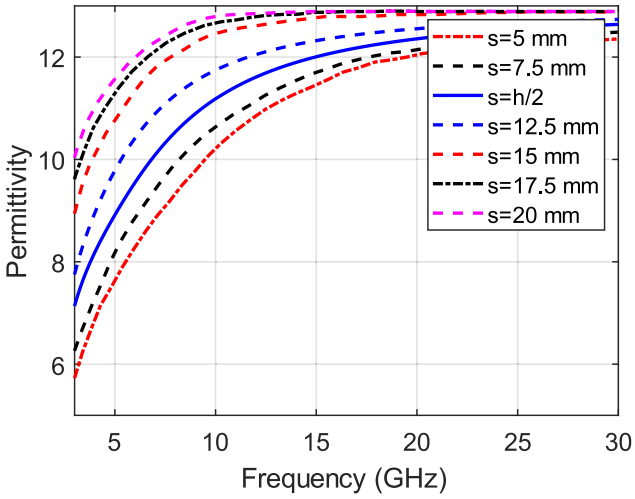

FIGURE 3. Parametric analysis of effective permittivity for different volumes of GaAs in the composite DRA.

It is observed that the effective permittivity is significantly influenced by variations in the volume of the GaAs based DR at the lower frequency resonance. However, as the frequency increases, the permittivity profiles converge to the high permittivity materials. Thus, the effective permittivity at high frequency is dominated by the GaAs material. At lower frequency bands, the composite DRA can be treated as a cylindrical DRA having ε_{eff}=7.67. The resonant frequency is approximated using (2). The value of the root X for cylindrical DRA, having inner to outer radius ratio b/a = 0, is 9.7. The resonant frequency is calculated to be 3.29 GHz. It is evident that the resonant frequency has reduced by a factor of 4.12 GHz. The inclusion of the high permittivity cylindrical DR plays a vital role in reducing the resonant frequency of the annular DRA to the desired resonant frequency which covers the n79 band of sub-6 GHz band of the 5G communication.

Electric field distribution for the dominant mode is presented in Fig. 4. Electric field lines are observed to be pointing outward from the central axis of DRA. This shows the excitation of the fundamental $TM_{01\delta}$ mode, producing a distribution similar to that of a half-wavelength monopole. The simulated results of the reflection coefficient for both annular and composite DRA are compared in Fig. 5. It can be observed that the annular DRA resonates at 7.56 GHz. Whereas, the composite DRA exhibits a resonance frequency of 4.44 GHz. The shift in the resonance frequency is observed by the factor of 3.1 GHz.

In the millimeter-wave frequency band, the wavelength becomes comparable to the antenna dimensions. Consequently, the conventional method of calculating effective permittivity through (3) loses its effectiveness. The cylindrical DRA is excited in the higher order modes to achieve mm-wave band resonance. Due to the composition of two distinct materials within the DRA, no closed-form solution exists for its analysis. Therefore, to anticipate the resonance frequency within the millimeter-wave band, CST's

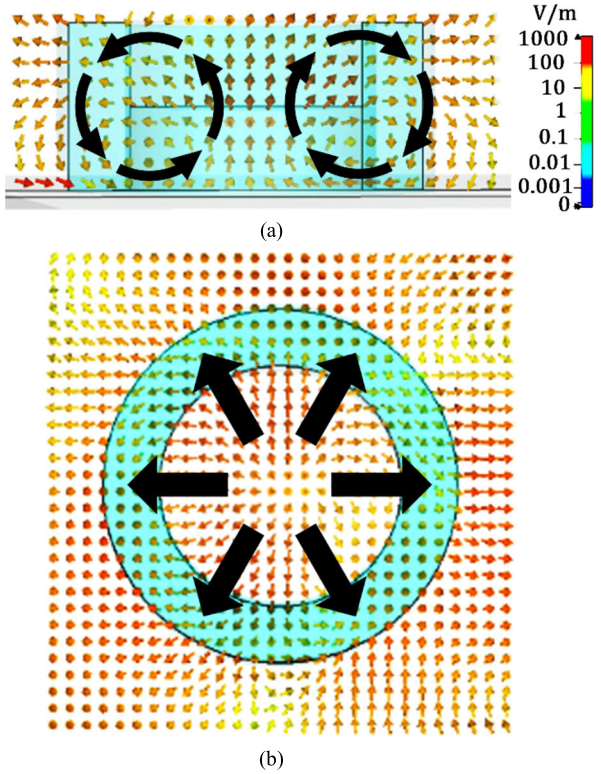

FIGURE 4. Electric field distribution in the composite DRA in (a) azimuthal and (b) radial axes.

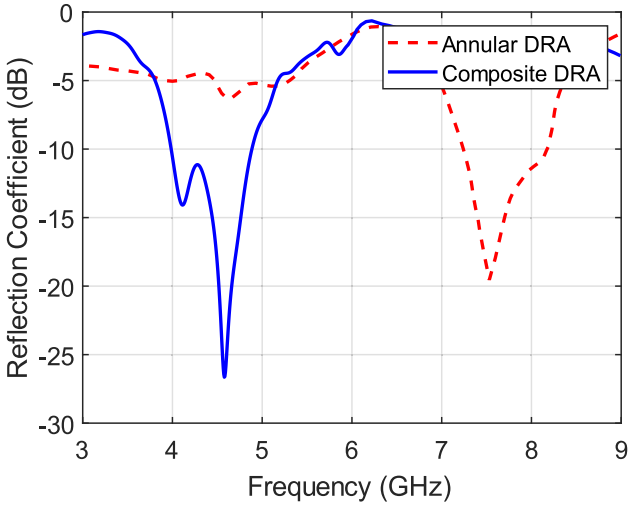

FIGURE 5. Reflection coefficients of the simulated annular DRA resonating at 7.56 GHz and composite DRA resonating at sub-6 GHz frequency band.

eigenmode solver was employed. The composite DRA exhibits resonance with three higher-order modes, namely $TM_{41\delta}$, $TM_{33\delta}$, and $TM_{14\delta}$.

C. FEED NETWORK DESIGN

In order to excite the annular marble DRA, a feeding mechanism is implemented using a co-planar waveguide (CPW) as shown in Fig. 1. This choice of CPW as the feeding

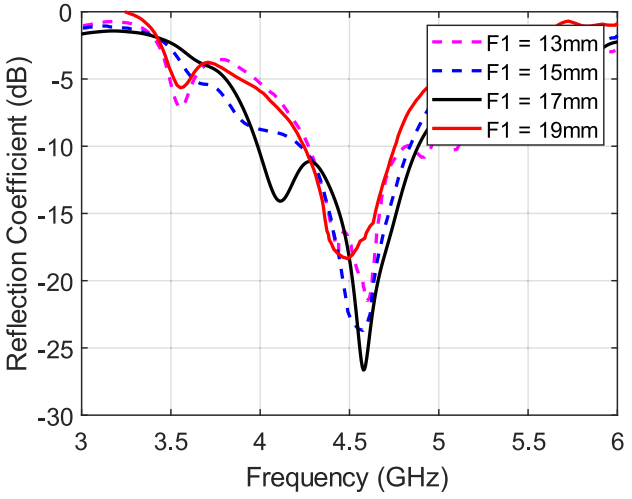

FIGURE 6. Parametric analysis of reflection coefficient for various lengths of CPW feed at sub-6 GHz band.

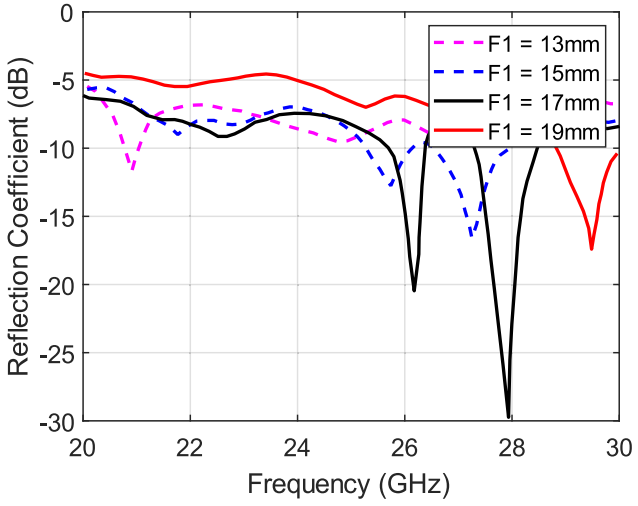

FIGURE 7. Parametric analysis of reflection coefficient for various lengths of CPW feed at mm-wave band.

mechanism offers several advantages, including a wide range of frequency bands and lower signal losses when compared to alternative feedline configurations such as microstrip and co-axial feedlines. Parametric analysis of the length of CPW feed is carried out to optimize the feeding position for the proposed DRA. Fig. 6 and Fig. 7 show the simulated results of the reflection coefficient for various values of the feed length F1. It is observed that the length of the CPW feed has a slight impact on the resonance of the proposed DRA. However, the length parameter significantly influences the impedance bandwidth of the DRA. The optimum feeding position to ensure maximum impedance bandwidth is obtained at F1 = 17 mm.

III. RESULTS AND DISCUSSION

The proposed DRA is fabricated using abrasive waterjet cutting. Fig. 8 shows the fabricated structure of the pro-

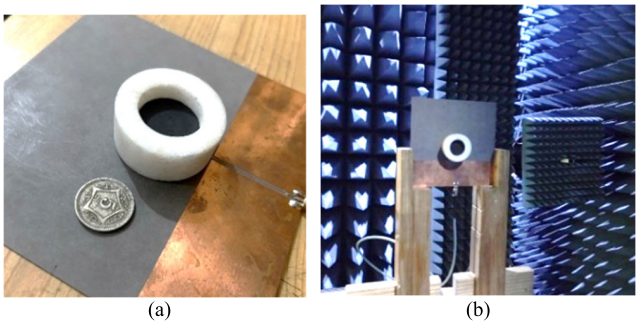

FIGURE 8. (a) Fabricated Prototype of the proposed DRA (b) Measurement of far-field radiation patterns in anechoic chamber.

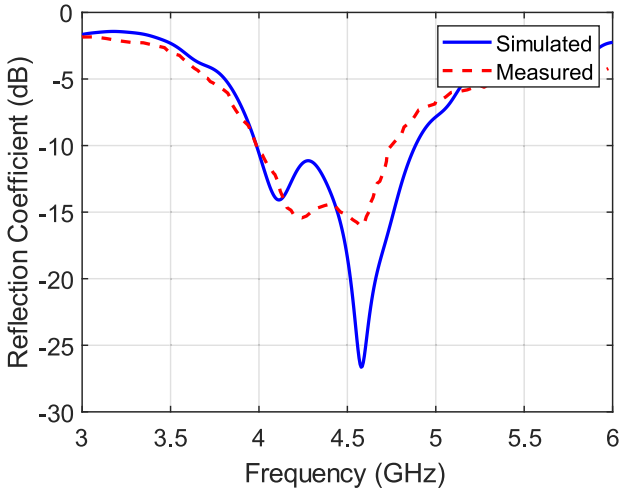

FIGURE 9. Measured and simulated reflection coefficient at sub-6 GHz frequency band.

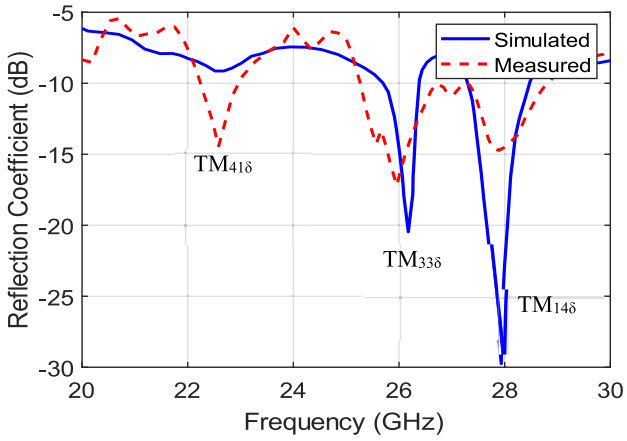

FIGURE 10. Measured and simulated reflection coefficient at mm-wave frequency band.

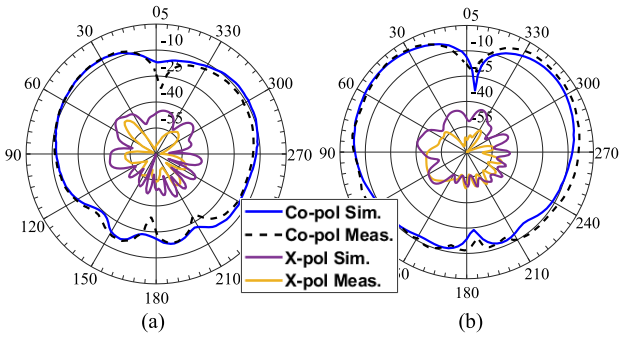

FIGURE 11. Far-field radiation patterns at 4.44 GHz (a) phi=0 plane, (b) phi=90 plane.

posed composite DRA. The measurement of the reflection coefficient was performed using Anritsu MS46122B vector network analyzer. Measurement of the far-field radiation patterns was performed in the anechoic chamber at the RF and microwave measurement facility at the National University of Science and Technology (NUST) for the verification of the results. Results of the simulated and fabricated composite DRA are described in the following sub-sections.

A. REFLECTION COEFFICIENT

The simulated and measured results of the reflection coefficient at sub-6 GHz band are presented in Fig. 9. The measured reflection coefficient is observed to align well with the simulated results. The proposed composite DRA offers impedance bandwidth of 880 MHz (4 GHz - 4.88 GHz) and a fractional bandwidth of 19.8%. The lower band of the proposed DRA covers n79 band of the 5G communication. The mm-wave band results of simulated and measured reflection coefficients are shown in Fig. 10. It is evident from the reflection coefficient profile that the composite DRA is excited at three higher order modes $TM_{41\delta}$, $TM_{33\delta}$ and $TM_{14\delta}$. The resonance at the latter two modes enables wide-band response having an impedance bandwidth of 1.16 GHz (27.34 GHz – 28.5 GHz) and fractional bandwidth is observed to be 4.1%. The mm-wave band of the proposed composite DRA covers the n261 band of the 5G network. It can be observed that the measured results closely match the simulated results.

B. FAR-FIELD RESULTS

The far-field radiation patterns of the simulated and fabricated composite DRA at 4.44 GHz are shown in Fig. 11. The co-polarization and cross-polarization radiation patterns are normalized with respect to the maximum value of co-polarization. The far-field radiations in the azimuthal and elevation axes are presented by the phi=0 and phi=90 planes respectively. The Half Power Beamwidth (HPBW) at the sub-6 GHz band is observed to be 65.23° in the azimuth plane and 55.15° in the elevation plane. The HPBW at the mm-wave band is 39° in the azimuth and 20.12° in the elevation plane. It is observed that the proposed DRA radiates in broad-side directions in both planes imitating the radiation characteristics of a half-wavelength monopole. The composite DRA exhibits peak gain of 6.8 dBi in the lower-band. The cross-polarization level is observed to be lower

TABLE 2. Comparison with the related work.

Ref	Antenna Type	Ports	Volume (cm^3/λ^3)	f_r (GHz)	Frequency Ratio	BW (%)	Gain (dBi)
[20]	DRA	2	0.017	5.15	5.9	21	6.4
	Dielectric Lens			30.5		26.2	12.7
[21]	DRA	2	0.014	2.72	9.3	38.2	6.5
	FPRA			25.3		16.2	11.3
[22]	DRA	2	0.025	2.73	8.9	30.8	8.23
	FPRA			24.4		4.7	17.2
[24]	Slot	2	3.393e-4	5.2	4.6	1.93	3.9
	SI-DRA			24		6.3	6.3
[23]	DRA	6	0.265	3.6	8.47	33	7.2
	DRA			30.5		27	18
[26]	DRA	1	0.011	1.87	1.36	25.3	6.09
				2.55		35.3	8.49
[18]	DRA	1	0.016	5.19	1.76	26.25	4.3
				9.13		11.17	5.8
This work	**DRA**	**1**	**0.1**	**4.44**	**6.28**	**19.8**	**6.8**
				27.92		**4.1**	**4.3**

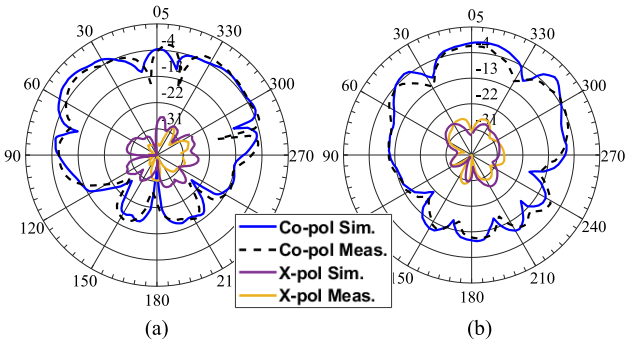

FIGURE 12. Far-field radiation patterns at 27.92 GHz (a) phi=0 plane, (b) phi=90 plane.

than -40 dBi. The far-field radiation patterns at 27.92 GHz, normalized to the maximum of co-polarization, are presented in Fig. 12. The peak gain at the mm-wave frequency band is 4.3 dBi and the cross-polarization level is less than −22 dBi. The composite DRA exhibits radiation efficiency of 87.1% and 84.71% in the sub-6 GHz and mm-wave bands respectively.

C. COMPARISON WITH THE STATE OF THE ART

The comparison between the proposed composite DRA and state-of-the-art antennas with large frequency ratios is shown in Table 2. Large-frequency ratio antennas presented in [20], [21], [22], [23], and [24] use a combination of multiple distinct radiating elements excited separately. Multi-port feeding mechanism is used to excite distinct radiators at both low-frequency and high-frequency bands. A combination of DRs is used in [20] for dual-band operation with large frequency ratio. A cylindrical DR and a dielectric lens (DL) are designed to resonate at sub-6GHz and a secondary smaller DR is embedded under the larger DR for mm-wave band resonance. The larger DR and DL act as radiating aperture at mm-wave band to enhance the gain and offer the pek gain of 12.7 dBi. However, the radiating efficiency at mm-wave band is 77% which is much less as compared to the proposed antenna. A similar combination of DL with smaller DRAs encapsulated inside a larger 3D-printed DRA was presented [23]. The sub-6 GHz DRA was excited using slot coupled feed and the encapsulated 5-element MIMO was excited using microstrip feed lines. Moreover, the 3D-printed DRA was excited with 6 ports resulting in a complex feeding network. On the other hand, the proposed DRA is singly-fed and is more than 50% smaller in size as compared to the 3D-printed DRA. MIMO configuration of the mm-wave band radiators offered an improved efficiency of 80% as compared to the earlier work [20]. A metallic groove on the top of rectangular DRA is used to offer mm-wave band resonance [21]. Apart from fabrication and integration complexity due to two distinct feeding approaches for sub-6 GHz and mm-wave band operations, the metallic radiator also suffers from low radiation efficiency at mm-wave band. The radiation efficiency at mm-wave band is 75% at its resonance frequency of 24 GHz. Whereas, the proposed composite DRA offers 84.71% efficiency in the upper band. A combination of DRA and FPRA was used for dual-band resonance at sub-6 GHz and mm-wave bands respectively. A feeding strip is used to excite the cylindrical DRA at sub-6 GHz band whereas a WR-34 waveguide is used for excitation at mm-wave band. The radiation characteristics at the mm-wave band depict a high gain of 17.2 dBi and efficiency of 87.3%. Though the antenna offers high gain and efficiency, the excitation method makes it less suitable for its integration with printed circuits limiting its applicability.

A combination of dual-fed slot antenna and substrate integrated DRA was used for dual-band operation with large frequency ratio [24]. The DRA was surrounded with metallic vias and air holes to achieve impedance matching and desired directivity. However, the air holes caused significant fabrication tolerance causing a reduction in realized radiation efficiency which was observed to be only 63% at sub-6 GHz band. On the other hand, the simplistic cylindrical nature of the proposed composite DRA makes it very unlikely to cause fabrication tolerance.

The dual-band large frequency-ratio antennas discussed above use multiple excitations for different frequency bands. It was observed that the antennas that utilize metallic radiating elements or combinations of DRA with DL suffer from conducting losses and tend to offer less efficiency. Moreover, the large-frequency- ratio antennas in the literature use a combination of different feeding mechanisms including waveguide, slot-coupled feed, metallic strip and microstrip feedlines making them less suitable for integration with other systems. Singly-fed antennas presented in [19] and [26] are based on single element radiators and offer dual-band resonance. However, the frequency ratio is much lesser as compared to the proposed composite DRA. The proposed DRA covers both the mid-band and the mm-wave band of the 5G network utilizing a single CPW feed. The fractional bandwidth at the mm-wave band is narrower as compared to the bandwidth in the sub-6 GHz due to the higher order resonance. Moreover, the presence of spurious resonant modes contributes to narrowing the fractional bandwidth in the mm-wave band. The antenna exhibits good radiation characteristics having higher efficiency as compared to the state-of-the-art.

IV. CONCLUSION

A novel and efficient composite DRA is proposed in this article. The composite DRA is designed to offer dual-band resonance for 5G applications. The proposed dual-band composite DRA consists of a singly-fed annular dielectric structure and a high permittivity DR embedded concentrically. CPW feeding method is used to excite the fundamental mode ($TM_{01\delta}$) for resonance in sub-6 GHz, and higher-order modes ($TM_{41\delta}$, $TM_{33\delta}$, and $TM_{14\delta}$) for mm-wave resonance. The performance of the proposed composite DRA was optimized by carrying out the parametric analysis considering the parameters of the CPW feed and the volume of dielectric structures. The prototype of the composite DRA was fabricated through water-jet cutting method. The prototype of the DRA was tested and the results were compared to the simulated ones. The measured results demonstrate that the proposed antenna achieved dual-band resonance at 4.44 GHz with the fundamental resonant mode $TM_{01\delta}$ and 27.92 GHz with higher order mode. Additionally, the antenna demonstrated high efficiency, broadside radiation patterns, and substantial fractional bandwidth. The single-port CPW feed enables the proposed antenna to be conveniently integrated with numerous underlying systems. The dual-band large frequency ratio resonance makes the proposed DRA a promising choice for a variety of 5G applications including eMBB, mMTC, URLLC, and FWA.

REFERENCES

[1] T. S. Rappaport, J. N. Murdock, and F. Gutierrez, "State of the art in 60-GHz integrated circuits and systems for wireless communications," *Proc. IEEE*, vol. 99, no. 8, pp. 1390–1436, Aug. 2011.
[2] Z. Pi and F. Khan, "An introduction to millimeter-wave mobile broadband systems," *IEEE Commun. Mag.*, vol. 49, no. 6, pp. 101–107, Jun. 2011.
[3] F. Gutierrez, S. Agarwal, K. Parrish, and T. S. Rappaport, "On-chip integrated antenna structures in CMOS for 60 GHz WPAN systems," *IEEE J. Sel. Areas Commun.*, vol. 27, no. 8, pp. 1367–1378, Oct. 2009.
[4] T. S. Rappaport, E. Ben-Dor, J. N. Murdock, and Y. Qiao, "38 GHz and 60 GHz angle-dependent propagation for cellular & peer-to-peer wireless communications," in *Proc. IEEE Int. Conf. Commun. (ICC)*, Jun. 2012, pp. 4568–4573.
[5] Y. Azar, G. N. Wong, K. Wang, R. Mayzus, J. K. Schulz, H. Zhao, F. Gutierrez, D. Hwang, and T. S. Rappaport, "28 GHz propagation measurements for outdoor cellular communications using steerable beam antennas in new York city," in *Proc. IEEE Int. Conf. Commun. (ICC)*, Jun. 2013, pp. 5143–5147.
[6] D. Wang and C. H. Chan, "Multiband antenna for WiFi and WiGig communications," *IEEE Antennas Wireless Propag. Lett.*, vol. 15, pp. 309–312, 2016.
[7] B. J. Xiang, S. Y. Zheng, H. Wong, Y. M. Pan, K. X. Wang, and M. H. Xia, "A flexible dual-band antenna with large frequency ratio and different radiation properties over the two bands," *IEEE Trans. Antennas Propag.*, vol. 66, no. 2, pp. 657–667, Feb. 2018.
[8] R. Hussain, A. T. Alreshaid, S. K. Podilchak, and M. S. Sharawi, "Compact 4G MIMO antenna integrated with a 5G array for current and future mobile handsets," *IET Microw., Antennas Propag.*, vol. 11, no. 2, pp. 271–279, Jan. 2017.
[9] Z.-X. Xia, K. W. Leung, M. W. K. Lee, and N. Yang, "Miniature dual-band meander-line monopole chip antenna with independent band control," *IEEE Antennas Wireless Propag. Lett.*, vol. 18, pp. 1873–1877, 2019.
[10] K.-L. Wong, H.-J. Chang, C.-Y. Wang, and S.-Y. Wang, "Very-low-profile grounded coplanar waveguide-fed dual-band WLAN slot antenna for on-body antenna application," *IEEE Antennas Wireless Propag. Lett.*, vol. 19, pp. 213–217, 2020.
[11] S. Long, M. McAllister, and L. Shen, "The resonant cylindrical dielectric cavity antenna," *IEEE Trans. Antennas Propag.*, vol. AP-31, no. 3, pp. 406–412, May 1983.
[12] R. Kumar Mongia and A. Ittipiboon, "Theoretical and experimental investigations on rectangular dielectric resonator antennas," *IEEE Trans. Antennas Propag.*, vol. 45, no. 9, pp. 1348–1356, Sep. 1997.
[13] X. S. Fang and S. M. Chen, "Design of the wide dual-band rectangular souvenir dielectric resonator antenna," *IEEE Access*, vol. 7, pp. 161621–161629, 2019.
[14] P. Kumar, S. Dwari, M. K. Mandal, S. Singh, J. Kumar, A. Kumar, and Utkarsh, "Electronically controlled beam steerable dual-band star-shaped DRA for UAS and Wi-Fi data link applications," *IEEE Trans. Antennas Propag.*, vol. 68, no. 10, pp. 7214–7218, Oct. 2020.
[15] Y. X. Sun and K. W. Leung, "Dual-band and wideband dual-polarized cylindrical dielectric resonator antennas," *IEEE Antennas Wireless Propag. Lett.*, vol. 12, pp. 384–387, 2013.
[16] H. Tang, J.-X. Chen, W.-W. Yang, L.-H. Zhou, and W. Li, "Differential dual-band dual-polarized dielectric resonator antenna," *IEEE Trans. Antennas Propag.*, vol. 65, no. 2, pp. 855–860, Feb. 2017.
[17] X.-C. Wang, L. Sun, X.-L. Lu, S. Liang, and W.-Z. Lu, "Single-feed dual-band circularly polarized dielectric resonator antenna for CNSS applications," *IEEE Trans. Antennas Propag.*, vol. 65, no. 8, pp. 4283–4287, Aug. 2017.
[18] Y.-D. Zhou, Y.-C. Jiao, Z.-B. Weng, and T. Ni, "A novel single-fed wide dual-band circularly polarized dielectric resonator antenna," *IEEE Antennas Wireless Propag. Lett.*, vol. 15, pp. 930–933, 2016.
[19] M. Zhang, B. Li, and X. Lv, "Cross-slot-coupled wide dual-band circularly polarized rectangular dielectric resonator antenna," *IEEE Antennas Wireless Propag. Lett.*, vol. 13, pp. 532–535, 2014.

[20] R. S. Malfajani, H. Niknam, S. Bodkhe, D. Therriault, J.-J. Laurin, and M. S. Sharawi, "A dual wide-band mushroom-shaped dielectric antenna for 5G sub-6-GHz and mm-wave bands," *IEEE Open J. Antennas Propag.*, vol. 4, no. 1, pp. 614–625, Jul. 2023.

[21] L. Y. Feng and K. W. Leung, "Wideband dual-frequency antenna with large frequency ratio," *IEEE Trans. Antennas Propag.*, vol. 67, no. 3, pp. 1981–1986, Mar. 2019.

[22] L. Y. Feng and K. W. Leung, "Dual-fed hollow dielectric antenna for dual-frequency operation with large frequency ratio," *IEEE Trans. Antennas Propag.*, vol. 65, no. 6, pp. 3308–3313, Jun. 2017.

[23] R. S. Malfajani, H. Niknam, S. Bodkhe, D. Therriault, J.-J. Laurin, and M. S. Sharawi, "A 3D-printed encapsulated dual wide-band dielectric resonator antenna with beam switching capability," *IEEE Open J. Antennas Propag.*, vol. 4, pp. 492–505, 2023.

[24] Y.-X. Sun and K. W. Leung, "Substrate-integrated two-port dual-frequency antenna," *IEEE Trans. Antennas Propag.*, vol. 64, no. 8, pp. 3692–3697, Aug. 2016.

[25] A. Muhammad, M. U. Khan, R. S. Malfajani, M. S. Sharawi, and M. Alathbah, "An integrated DRA-based large frequency ratio antenna system consisting of a MM-wave array and a MIMO antenna for 5G applications," *IEEE Open J. Antennas Propag.*, vol. 5, no. 2, pp. 368–378, Apr. 2024.

[26] X. Fang, K. W. Leung, and E. H. Lim, "Singly-fed dual-band circularly polarized dielectric resonator antenna," *IEEE Antennas Wireless Propag. Lett.*, vol. 13, pp. 995–998, 2014.

[27] M. Bağci, "Mineralogical, petrographic, and geochemical characterization of colored iscehisar marbles (Afyonkarahisar, W-Turkey)," *Turkish J. Earth Sci.*, vol. 29, no. 6, pp. 946–975, Sep. 2020.

[28] I. Akdag, C. Gocen, M. Palandoken, and A. Kaya, "A novel circularly polarized reader antenna design for UHF RFID applications," *Wireless Netw.*, vol. 28, no. 6, pp. 2625–2636, Aug. 2022.

[29] K. M. Luk and K. W. Leung, *Dielectric Resonator Antennas*. Baldock, U.K.: Research Studies Press, 2003.

[30] G. N. Rocha, L. F. L. Melo, M. A. S. da Silva, P. V. S. Silva, A. S. B. Sombra, and P. B. A. Fechine, "Study of the performance of dielectric resonator antennas based on the matrix $BiREWO_6$ [RE=Gd, Y, Nd]," *Microw. Opt. Technol. Lett.*, vol. 54, no. 1, pp. 18–23, Jan. 2012.

[31] Y. Zhang, J.-Y. Deng, M.-J. Li, D. Sun, and L.-X. Guo, "A MIMO dielectric resonator antenna with improved isolation for 5G mm-wave applications," *IEEE Antennas Wireless Propag. Lett.*, vol. 18, pp. 747–751, 2019.

[32] P. Rajat Girjashankar and T. Upadhyaya, "Substrate integrated waveguide fed dual band quad-elements rectangular dielectric resonator MIMO antenna for millimeter wave 5G wireless communication systems," *AEU Int. J. Electron. Commun.*, vol. 137, Jul. 2021, Art. no. 153821.

[33] W. Mazhar, D. M. Klymyshyn, G. Wells, A. A. Qureshi, M. Jacobs, and S. Achenbach, "Low-profile artificial grid dielectric resonator antenna arrays for mm-wave applications," *IEEE Trans. Antennas Propag.*, vol. 67, no. 7, pp. 4406–4417, Jul. 2019.

[34] E. E. C. Oliveira, A. G. D'Assunção, J. B. L. Oliveira, and A. M. Cabral, "Small size dual-band rectangular dielectric resonator antenna based on calcium titanate ($CaTiO_3$)," *Microw. Opt. Technol. Lett.*, vol. 54, no. 4, pp. 976–979, Apr. 2012.

[35] U. Ullah, W. F. F. W. Ali, M. F. Ain, N. M. Mahyuddin, and Z. A. Ahmad, "Design of a novel dielectric resonator antenna using $MgTiO_3$-$CoTiO_3$ for wideband applications," *Mater. Design*, vol. 85, pp. 396–403, Nov. 2015.

[36] P. Tripathi, B. Sahu, S. P. Singh, O. Parkash, and D. Kumar, "Preparation and characterization of liquid phase ($55B_2O_3$–$45Bi_2O_3$) sintered cobalt doped magnesium titanate for wideband stacked rectangular dielectric resonator antenna (RDRA)," *Ceram. Int.*, vol. 41, no. 2, pp. 2908–2916, Mar. 2015.

[37] S. Pandey, D. Kumar, O. Parkash, and L. Pandey, "Design and development of dielectric resonator antenna using ceramic materials: An overview," *Trans. Indian Inst. Met.*, vol. 72, no. 8, pp. 2019–2028, Aug. 2019.

[38] J.-G. Hyun, S. Lee, S.-D. Cho, and K.-W. Paik, "Frequency and temperature dependence of dielectric constant of Epoxy/$BaTiO_3$ composite embedded capacitor films (ECFs) for organic substrate," in *Proc. Electron. Compon. Technol., ECTC.*, 2005, pp. 1241–1247.

[39] H. F. Ma and T. J. Cui, "Three-dimensional broadband and broad-angle transformation-optics lens," *Nature Commun.*, vol. 1, no. 1, pp. 1–7, Nov. 2010.

[40] K. Y. You, "Materials characterization using microwave waveguide systems," in *Microwave Systems and Applications*. Rijeka, Croatia: IntechOpen, 2017, pp. 341–357.

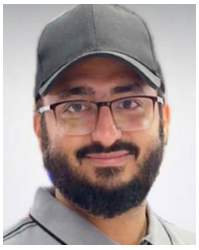

ASADULLAH received the B.S. degree in electrical (telecommunication) engineering from COMSATS University, Islamabad, Pakistan, in 2012, and the M.S. degree in computer communication and networks from Sukkur IBA University, Sindh, Pakistan, in 2017. He is currently pursuing the Ph.D. degree in electrical engineering with the National University of Science and Technology (NUST), Islamabad.

From 2014 to 2015, he was a Research Assistant with the Department of Mathematics, Sukkur IBA University. He is currently a Lecturer with the Department of Telecommunication Engineering, Quaid-e-Awam University of Science and Technology, Nawabshah, Pakistan. His research interests include the design and characterization of multi-band dielectric resonator antennas, digital signal processing, and employing deep learning techniques for biometric identification systems.

MUHAMMAD UMAR KHAN (Member, IEEE) received the M.S. degree in electrical engineering from the Ghulam Ishaq Khan Institute of Engineering Sciences and Technology, Topi, Pakistan, in 2008, and the Ph.D. degree in electrical engineering from the King Fahd University of Petroleum and Minerals, Dhahran, Saudi Arabia, in 2015. He is currently an Associate Professor with the School of Electrical Engineering and Computer Science, National University of Sciences and Technology, Islamabad, Pakistan. His research interests include printed antennas and antenna arrays, MIMO antenna systems, and reconfigurable antennas.

AWAB MUHAMMAD received the B.S. and M.S. degrees in electrical engineering from the National University of Sciences and Technology (NUST), Islamabad, Pakistan, in 2018 and 2023, respectively.

His research interests include reflectarrays, transmit arrays, multi-beam antennas, DRAs, microstrip patch antennas, large frequency ratio antennas, and higher-order mode antennas.

MOHAMMAD S. SHARAWI (Fellow, IEEE) received the M.Sc. and Ph.D. degrees from Oakland University, Rochester, MI, USA, in 2002 and 2006, respectively.

From 2019 to 2023, he was a Full tenured Professor (Professeur Titulaire) of electrical engineering with Polytechnique Montréal, Montreal, QC, Canada. From 2009 to 2018, he was with the King Fahd University of Petroleum and Minerals (KFUPM), Dhahran, Saudi Arabia, where he founded and directed the Antennas and Microwave Structure Design Laboratory (AMSDL). He was a Visiting Professor with the Intelligent Radio Laboratory (iRadio), Department of Electrical Engineering, University of Calgary, Calgary, AB, Canada, in Summer–Fall 2014. He was a Visiting Research Professor with Oakland University, Rochester, MI, USA,

in 2013 and 2023. He is currently a Principal Engineer at Blue Origin LLC, Kent, WA, USA, working on research and development projects for space communication systems. He is also a Professor with the Department of Electrical and Computer Engineering, University of Washington, Seattle, WA, USA. He has more than 400 papers published in refereed journals and international conferences, 11 book chapters, two of which in the *Antenna Handbook* (fifth edition, McGraw Hill, 2018), one single-authored book titled *Printed MIMO Antenna Engineering* (Artech House, 2014), the Lead Author of the book *Design and Applications of Active Integrated Antennas* (Artech House, 2018), and a coauthor of the book *MIMO Antenna Systems for 5G and Beyond* (IEEE-Wiley, 2024). He has 28 issued/granted and ten pending patents in the U.S. Patent Office. His research interests include multiband printed multiple-input–multiple-output (MIMO) antenna systems, reconfigurable and active integrated antennas, millimeter-wave antennas, integrated 4G/5G and beyond 5G antenna systems, shared aperture and encapsulated antennas, microwave sensors, applied electromagnetics, sub-THz structures, and computational methods. He is a fellow of IET. He was a recipient of the Abdul Hameed Shoman Foundation Award for Arab Researchers for the category of wireless systems, in 2020, in addition to various best IEEE conference paper awards. He has served on the Technical and Organizational Program Committees as well as organized several special sessions on MIMO antenna systems and their applications in 4G and 5G wireless systems in several international conferences, such as European Conference on Antennas and Propagation (EuCAP), Antennas and Propagation Society (APS), International Microwave Workshop Series on 5G Hardware and System Technologies (IMWS-5G), Asia-Pacific Conference on Antennas and Propagation (APCAP), International Workshop on Antenna Technology (iWAT), among many others for many years. He has served as the IEEE APS Chair for the Montreal Section (2020–2023) and an Active Member of the IEEE Member Benefits Committee leading the initiative of the APS Student Travel Grant. He is also the Regional Delegate of the EuRAAP in North America. He was an Associate Editor of IEEE Antennas and Wireless Propagation Letters, from 2019 to 2023. He was the Specialty Chief Editor of the newly launched *Frontiers in Communications and Networks* for the System and Test-Bed Design Section, from 2020 to 2022. He has been serving as an Associate Editor for the IEEE Open Journal of Antennas and Propagation and *IET Microwaves, Antennas and Propagation* (Wiley), and an Area Editor (antennas and microwave devices and systems) for *Microwave and Optical Technology Letters* (Wiley) since 2020. He is a Distinguished Lecturer (DL) for APS, from 2023 to 2025. He is currently serving as the AP/MTT/ED Seattle Joint Chapter Co-Chair.

MOATH ALATHBAH received the Ph.D. degree from Cardiff University, U.K. He is currently an Assistant Professor with King Saud University, Saudi Arabia. His research interests include the development of photoelectronic, integrated electronic active and passive discrete devices, the design, fabrication, and characterization of MMIC, RF, and THz components, smart antennas, microstrip antennas, microwave filters, meta-materials, 5G antennas, MIMO antennas miniaturized multiband/wideband antennas, and microwave/millimeter components using micro and nano technology.